Integration of thalamic and retrosplenial inputs in presubicular layer 3 gates cross-laminar bursting signal to upstream head direction circuit

Authors

Louis Richevaux[1]*, Dongkyun Lim[1], Mérie Nassar[1], Constanze Mauthe[1], Ivan Cohen[3], Nathalie Sol-Foulon[2], Desdemona Fricker[1]*

[1]Université Paris Cité, CNRS, Integrative Neuroscience and Cognition Center, F-75006 Paris, France, [2]Sorbonne Université, INSERM, CNRS, Paris Brain Institute, ICM, Pitié-Salpêtrière Hospital, F-75013 Paris, France, [3]Sorbonne Université, INSERM, CNRS, Neuroscience Paris Seine, Institut de Biologie Paris Seine, F-75005 Paris, France

Correspondence: desdemona.fricker@parisdescartes.fr, louis.richevaux@parisdescartes.fr

Visual abstract

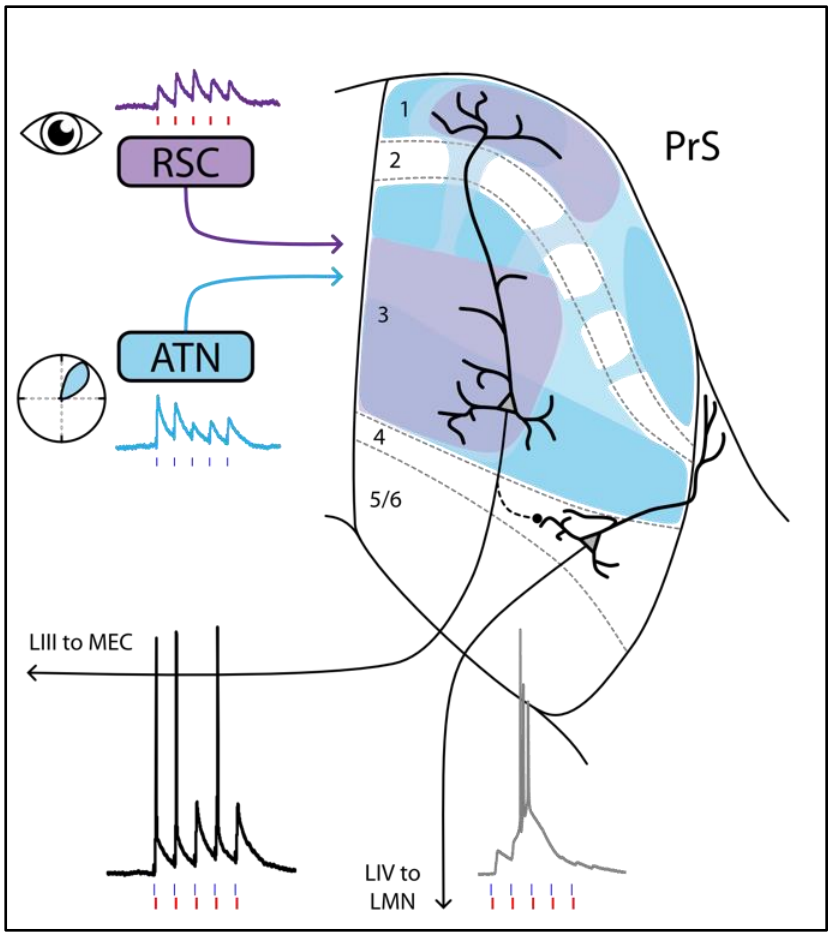

Abstract

Head-direction (HD) signals function as the brain's internal compass. They are organized as an attractor, and anchor to the environment via visual landmarks. Here we test the hypothesis that HD and landmark signals are associated in the dorsal presubiculum. We find that monosynaptic excitatory connections from anterior thalamic nucleus and from retrosplenial cortex converge on single layer 3 presubicular neurons. Independent dual wavelength photostimulation of these inputs in slices leads to action potential generation preferentially for near-coincident inputs, sending an integrated HD signal to medial entorhinal cortex. Layer 4 neurons, which innervate the lateral mammillary nucleus, form a second step in the association of HD and landmark signals. They are not directly contacted by thalamic and retrosplenial axons. Instead, layer 4 neurons receive a di-synaptic excitation from layer 3, providing a distinct landmark updating of HD signals for transmission to the lateral mammillary nucleus. Thus, a coherent sense of orientation involves projection specific translaminar processing in the presubiculum.

Introduction

The head direction (HD) system functions as the brain's compass system. It is distributed the head direction (HD) system functions as the brain's compass system. It is distributed across several interconnected brain structures, and hierarchically organized from the brainstem to the lateral mammillary nucleus (LMN; Stackman and Taube, 1998), the anterior thalamic nuclei (ATN; Taube, 1995), and the dorsal Presubiculum (PrS; Ranck, 1984; Taube et al., 1990). Modeling work suggests the HD system functions as a ring attractor, where the population of HD neurons is arranged in a one dimensional manifold (Blair and Sharp, 1995; McNaughton et al., 2006; Skaggs et al., 1995). The activity of thalamic and PrS HD neurons is correlated across different brain states, even during sleep, independently of sensory cues (Peyrache et al., 2015). The bump-like activity dynamics of an attractor network can maintain HD signals based on excitatory-excitatory or excitatory-inhibitory interactions (Knierim and Zhang, 2012; Simonnet et al., 2017). However, HD signals may drift in the dark (Taube et al., 1990b; Zugaro et al., 2003). For precise navigation, internally generated information on head direction must be combined with awareness of location in an environment. Mechanisms underlying the combination of egocentric head direction signals with anchoring to allocentric landmarks remain to be clarified.

Head direction and visual landmark signals may be integrated in the presubiculum (Jeffery et al., 2016; Yoder et al., 2019). Head direction cells are found in the superficial and deep layers of dorsal presubiculum, also termed postsubiculum (Boccara et al., 2010), and most layer 3 neurons in the dorsal presubiculum are head direction cells (Preston-Ferrer et al., 2016). These cells receive monosynaptic head direction inputs from the anterior thalamus (Nassar et al., 2018; Peyrache et al., 2015; Balsamo et al., 2022). Lesions of the PrS impair the visual landmark control of a cell's preferred direction in ATN and in LMN (Goodridge and Taube, 1997; Yoder et al., 2015). Presubicular lesions also induce place field instability in the hippocampus (Calton et al., 2003), suggesting this region may be crucial to the anchoring of directionally modulated neurons to environmental landmarks.

Landmark based navigation depends on reliable visual cues. The PrS appears to receive direct projections from the primary visual cortex and indirect visual input via the retrosplenial cortex (Van Groen & Wyss 2003; Vogt & Miller 1983). The retrosplenial cortex encodes angular head velocity (Alexander & Nitz 2015; Keshavarzi et al. 2022) and visual landmark information (Auger, Mullally, et Maguire 2012; Clark et al. 2010; Sit and Goard 2022). In particular, neurons in the dysgranular retrosplenial cortex encode landmark-dominated head-direction signals (Jacob et al., 2017). Presubicular layer 3 cells receiving projections from both the anterior thalamus and the retrosplenial cortex (Kononenko and Witter 2012) could update the compass and bind landmarks to head direction signals. Presubicular neurons could then broadcast integrated HD-landmark signals directly to the MEC, via deep layers to the ADN and via layer 4 neurons to the LMN (Huang et al., 2017; Yoder et al., 2015; Yoder and Taube, 2011). The different target-specific presubicular projection neurons are well positioned to integrate anterior thalamic and retrosplenial inputs, but technical constraints have limited understanding of how known anatomical inputs are transformed into functional integrated output signals.

This work was therefore designed to examine integration of visual landmarks and head direction signals in the PrS. Retrograde tracing was used to confirm inputs to the PrS from the ATN and the RSC. The spatial distribution of ATN and RSC targets in the dorsal and ventral PrS was investigated by stereotaxic injection of viral vectors inducing anterograde expression of light-gated ion channels fused to fluorescent reporters. We found that superficial layers of the dorsal PrS are major targets of ATN and RSC projections. We analyzed functional convergence of these inputs in the PrS using dual-wavelength optogenetic stimulations in ex vivo brain slices, while recording from layer 3 and 4 pyramidal neurons. Both ATN and RSC projections made mono-synaptic excitatory connections with single layer 3 principal cells and mostly di-synaptic ones with layer 4 cells. We show that EPSPs induced with close to coincident timing by ATN and RSC fibers summed non-linearly in layer 3 neurons. These data provide insights into the integration of landmark and head direction inputs and their distribution to downstream targets by PrS pyramidal cells.

Methods

KEY RESOURCES TABLE

REAGENT or RESOURCE	SOURCE	IDENTIFIER
Bacterial and virus strains		
AAV5.Syn.Chronos-GFP.WPRE.bGH	Addgene	59170P
AAV5.Syn.ChrimsonR-tdTomato.WPRE.bGH	Addgene	59171P
pAAVretro-CAG-tdTomato	Addgene	59462P
Chemicals, peptides, and recombinant proteins		
Retrobeads	Lumafluor	Red Retrobeads™
Streptavidin, Alexa Fluor™ 647 Conjugate	Thermofisher Scientific	S32357
Experimental models: Organisms/strains		
C57BL/6J	Janvier Labs	https://janvier-labs.com/fiche_produit/2-c57bl-6jrj/
Software and algorithms		
MATLAB	MathWorks	https://www.mathworks.com/
pClamp	Molecular devices	RRID:SCR_011323
AxoGraphX	Axograph	https://axograph.com
Other		
Prolong Gold antifade mountant	Invitrogen	Cat#P36930; RRID:SCR_015961

RESOURCE AVAILABILITY

Lead contact

Further information and requests should be directed to the lead contact, Desdemona Fricker (desdemona.fricker@parisdescartes.fr).

Materials availability

This study did not generate new, unique reagents.

EXPERIMENTAL MODEL AND SUBJECT DETAILS

Animals

Experiments were performed on wild-type and transgenic C57Bl6 mice, housed on a 12 hours

light/dark cycle with food and water available *ad libitum*. Animal care and use conformed to the European Community Council Directive (2010/63/EU) and French law (87/848). Our study was approved by the local ethics committee (CEEA - 34) and the French Ministry for Research 01025.02.

METHOD DETAILS

Viral vectors and beads

Projecting neurons were labeled with retrograde fluorescent tracers (Retrobeads, Lumafluor, and pAAV-CAG-tdTomato, Addgene 59462P). Fluorescent beads were stored at 4°C before use. Channelrhodopsin expression was achieved by injecting Adeno-associated viral constructions. AAV5.Syn.Chronos-GFP.WPRE.bGH (AAV5-Chronos, Penn Vector Core, Addgene 59170P) was used to induce neuronal expression of the blue light induced channelrhodopsin Chronos fused to the GFP marker and under the control of the Synapsin promoter. AAV5.Syn.ChrimsonR-tdTomato.WPRE.bGH (AAV5-Chrimson, Penn Vector Core, Addgene 59171P) induced neuronal expression of the red light gated channelrhodopsin Chrimson fused to the tdTomato marker, under the control of the Synapsin promoter. Viral vectors were stored at -80°C before use.

Stereotaxic surgery

Mice at ages of 4-5 weeks were anesthetized by intraperitoneal (i.p.) injection of a mixture of ketamine hydrochloride and xylazine (100 and 15 mg/kg respectively, in NaCl 0.9%). They were placed in a stereotaxic frame for injections. Fluorescent beads for retrograde tracing were injected (300-500 nl) into the PrS at the coordinates: -4.06 antero-posterior (AP), 2.00 medio-lateral (ML) and -2.15 mm dorso-ventral (DV) and into the LMN (-2.8 AP, 0.75 ML, -5.35 DV) with respect to the bregma.
Viral injections were performed unilaterally (Mathon et al., 2015; Richevaux et al., 2019) at the coordinates -0.82 AP, 0.75 ML and -3.2 mm DV for the ADN, and at -2.1 to -2.15 AP, 0.65 ML and -0.65 mm DV for the RSC. Volumes of 200 to 250 nl were injected with a 10 µL Hamilton syringe equipped with 33ga needle over a time of 10 min. The needle was slowly removed after a delay of 10 min to avoid leakage from the injection site. Best expression of AAV5 serotypes was achieved after 3 to 4 weeks.

Tissue fixation and slicing for retrograde tracing

Brains were removed for anatomy at 4 days after retrobead injection. Mice were anesthetized by i.p. injection of the ketamine/xylazine mixture. An intracardiac perfusion with 0.1M PBS was followed by perfusion with 4% paraformaldehyde. Brains were stored overnight in paraformaldehyde at 4°C and then washed in PBS. Coronal or horizontal sections were cut at 100 µm with a vibratome and stored in sucrose at 4°C.

Preparation of brain slices for physiology

Slices of the temporal lobe were prepared 3-4 weeks after injection of AAV5 viral constructions. Mice were anesthetized by i.p. injection of the ketamine/xylazine mixture. They were then perfused intracardially with a cutting solution containing (in mM): 125 NaCl, 25 sucrose, 2.5 KCl, 25 $NaHCO_3$, 1.25 NaH_2PO_4, 2.5 D-glucose, 0.1 $CaCl_2$, 7 $MgCl_2$, cooled to 4°C, and oxygenated with a 5% CO_2 / 95% O_2. The brain was removed and a vibratome was used to cut horizontal slices at 300 µm in the same solution. Slices were stored for 15 min at 34°C in an ACSF containing (in mM): 124 NaCl, 2.5 KCl, 26 $NaHCO_3$, 1 NaH_2PO_4, 2 $CaCl_2$, 2 $MgCl_2$, and 11 D-glucose, bubbled with 5% CO_2 / 95% O_2. They

were then kept in the same solution at room temperature until recording.

Whole-cell patch-clamp recordings

Slices were transferred to a recording chamber perfused with oxygenated, warmed (~32 °C) ACSF mounted on an epifluorescence microscope. Patch-clamp records were made from neurons with borosilicate glass pipettes of external diameter 1.5 mm (Clark Capillary Glass, Harvard Apparatus) pulled with a Brown-Flaming electrode puller (Sutter Instruments). Electrodes, filled with a potassium-gluconate based solution containing (in mM): 135 K-gluconate, 1.2 KCl, 10 HEPES, 0.2 EGTA, 2 $MgCl_2$, 4 MgATP, 0.4 Tris-GTP and 10 Na_2-phosphocreatine, had a resistance of 4-8 MΩ. An alternative, cesium-gluconate based solution facilitated neuronal depolarization to examine synaptic inhibition. It contained (in mM): 125 Cs-gluconate, 10 HEPES, 0.2 EGTA, 2 $MgCl_2$, 4 MgATP, 0.4 Tris-GTP and 10 Na_2-Phosphocreatine, together with 5 mM QX-314 to block Na^+ channels. Pipette solutions also contained 3 mM biocytin to reveal morphology after recording. They were adjusted to pH 7.3 and osmolarity 290 mOsm. Whole-cell, patch-clamp signals were filtered at 3kHz, amplified with a MultiClamp 700B amplifier and acquired with pCLAMP software (Molecular Devices). Monosynaptic excitation induced by optical stimulation was tested in the presence of TTX (1 µM) and 4-AP (100 µM). NBQX (10 µM) and APV (100 µM) were used to block AMPA and NMDA receptors respectively. Gabazine (10 µM) was used to block $GABA_A$ receptors.

Optical stimulation

LED illumination (Cairn Research, OptoLED) was used to visualize the fluorescent reporters GFP and tdTomato, and to stimulate opsin-expressing axons, using a 470 nm LED for Chronos and a 627 nm LED for Chrimson. Illuminated spots had a diameter of 200 µm with a 60x objective and were centered on the recorded cell soma. Photostimulation thus covered most of the basilar dendrites of layer 3 pyramidal neurons (typical distance from tip of apical to tip of basilar dendrite <400µm). Stimuli consisted of light pulses of 0.5 to 5 ms duration, repeated 5-10 times at 20 Hz.

A multiband filter allowed simultaneous stimulation by blue and red LEDs of axons containing Chronos and Chrimson (Simonnet et al., 2021). Stimulus power intensity (set in mV) was calibrated as light intensity. The response probability of layer 3 cells was calibrated to blue or red illumination of ATN or RSC afferents expressing Chronos or Chrimson to avoid stimulus overlap (see Supp. Fig. 5, 6). Chronos was targeted to the ATN and Chrimson to the RSC after testing the reverse configuration. Projections from the thalamus are larger and Chronos is more sensitive to blue light, so this configuration assured reliable activation of thalamic fibers at minimal blue-light intensities. For experiments investigating the integration of ATN and RSC inputs, we aimed to give similar weights to both inputs: Chrimson-expressing fibers were stimulated with light of intensity adjusted to initiate optically evoked excitatory postsynaptic potentials (oEPSPs) of amplitude similar to those induced by blue light Chronos-fiber stimuli.

Data analysis

ATN and RSC projections to the PrS, were analyzed from Chronos and Chrimson expression, using the ImageJ Plot Profile plug-in to quantitate normalized plot profiles (2000 pixels) of horizontal presubicular sections. Dorso-ventral differences were derived by dividing differences in labeling intensity between the PrS and the dentate gyrus (DG) molecular layer by DG intensity in slices from 5 dorso-ventral PrS levels. Values from all animals were averaged and then normalized.

Cells were qualified as synaptically ‘connected’ when they responded to light stimulation of

afferent axons with a delay < 8 ms. Slices with very low or absent expression of the fluorescent reporter were excluded. Cells were qualified as 'non-connected' synaptically, if they did not respond to light stimulation, but at least one neighboring cell in the same slice did.

Intrinsic neuronal properties were analyzed with custom MATLAB routines to derive 15 electrophysiological parameters (Huang et al., 2017). Parameters were standardized and unsupervised cluster analysis performed with MATLAB was used to compare different neurons (Huang et al., 2017; Simonnet et al., 2013).

Axograph was used to analyze responses to optical stimulation of ATN and RSC fibers. Layer 3 neurons were recorded at potentials near -65 mV. Responses to light were averaged from 10 stimulus trains at 20 Hz. Amplitudes and latencies of initial light evoked EPSCs, of latency shorter than 10ms, were quantified from voltage-clamp records. Latency was measured from stimulus onset to 10% of the peak amplitude of the first optically induced EPSC. Amplitude was measured with respect to the pre-stimulus baseline. Paired-pulse ratio (PPR) was defined as the ratio of the amplitude of the second to the first EPSC and 10/1 ratio as that between the 10th and the 1st EPSC, in responses to 20 Hz stimulations. Spike probability was counted over 5 to 10 trials per cell and then averaged over all cells. EPSPs induced by dual wavelength stimulation were analyzed using Axograph and a custom-made software. Events evoked by light stimuli were detected in a window of 1-10 ms after stimulation. EPSP amplitude and integrated area were calculated over 50 ms after stimulation. Baseline suppression was applied using an average of membrane potential during 50 ms before stimulation. Summation of ATN and RSC evoked EPSCs in layer 3 neurons was determined from the amplitude and integral of averaged events. Summation was considered to be supralinear, if values were more than 10% higher than a linear addition, linear for values within ± 10%, and sublinear for values more than 10% lower.

Biocytin revelation and morphology

Recorded neurons were filled with biocytin to visualize their morphology and location. Slices were fixed in 4% PFA in 0.1 M PBS at 4°C overnight, washed 3 times in 0.1 PBS and cryoprotected in 30% sucrose. Cell membranes were permeabilized by three freeze-thaw cycles over dry ice and rinsed in PBS. Slices were agitated in a saturation buffer (2% milk, 1% Triton X-100 in 0.1 M PBS) for 2 hours at room temperature. They were then incubated with Streptavidin-Cy5 conjugate (1:500) and DAPI (1:1000) overnight at 4°C. Sections were washed 3 times with PBS and mounted on coverslips with ProLong gold antifade mountant. For anatomical study they were mounted in Mowiol medium. Cell, bead and virus expression were visualized with an epifluorescence microscope. Higher resolution of morphology was obtained with confocal microscopy. The cell shown in Fig. 4 was reconstructed with Neurolucida software and those in Fig. 7 using IMARIS.

QUANTIFICATION AND STATISTICAL ANALYSIS

Data was analyzed with AxoGraphX and custom-written software (MATLAB, The MathWorks). Results are given as mean ± SEM. Statistical analysis was performed with Prism (GraphPad Software). The Mann-Whitney unpaired t-test was used to compare two groups. The Wilcoxon or Kruskal-Wallis test was used to compare paired groups. Evolution of parameters evoked by optical stimulation (current or potential amplitudes, spike probability) was analyzed with Friedman's test followed by multiple comparison Dunn's test. Šidák's multiple comparison test was also used to compare linear and observed responses to ATN and RSC stimulations. Significance levels are given as p values.

Results

ATN and RSC send strong axonal projections to the dorsal Presubiculum

The origins of the main afferents projecting to the presubiculum were explored by injecting retrogradely transported fluorescent beads into the PrS (Fig. 1A). After 4 days, coronal slices were prepared to examine the injection site and transport of the beads. Some beads remained close to the PrS injection site, due in part to local projections. Strong bead signals were detected within the two subnuclei that form the anterior thalamus, the anterodorsal (AD) and anteroventral (AV) part of ATN. Neurons in AD were labeled most strongly in the medial portion of the AD, while labeled neurons in AV were found in its lateral portion (Fig. 1B). Many neurons in the RSC were labeled. Cells with somata in layers 2 and 5 of the dysgranular dRSC were labeled, while mostly layer 5 cells of granular gRSC contained beads (Fig. 1C). Regions adjacent to the presubiculum including the subiculum (Sub), parasubiculum (PaS) and the medial and lateral entorhinal cortices (MEC, LEC) were labeled as was the contralateral PrS. Beads were also detected in the laterodorsal thalamic nucleus (LD). Table S1 summarizes these data, indicating some labeling also in the visual cortices, perirhinal cortex, the nucleus reuniens of the thalamus, the dorsolateral geniculate nucleus, and the claustrum. Some beads were observed in the CA1 region, which has not previously been reported. Potentially though, this labeling could derive from a bead leak into the nearby PaS which is innervated by CA1 (Van Groen et Wyss 1990a). In summary, the ATN and RSC are the major sources of afferents projecting to the presubiculum with lesser inputs from other sites.

Projections from the ATN or RSC to the presubiculum were explored by injecting at these sites an anterogradely transported viral construct which expressed the modified Channelrhodopsin Chronos fused to GFP (Fig. 1D). After 4 weeks, horizontal slices were prepared to verify the ATN injection site. Chronos-GFP labeling was mostly confined to the ATN, occasionally extending to medial thalamic and reticular nuclei nearby, possibly as bundles of projecting fibers (Fig. 1E, Supp. Fig. 1). After injection at the RSC site, coronal sections (Fig. 2F) showed strong expression in layer 5, especially deeper zones, and layer 6 of both dysgranular and granular RSC, while labeled dendrites were evident in layer 1. Chronos-GFP expression extended throughout the RSC, from -1.7 to -3.7 posterior to Bregma on the antero-posterior axis (Supp. Fig. 2).

Projections of the ATN to the presubiculum were examined in horizontal sections (Fig. 1G). ATN axons expressing the Chronos-GFP construct targeted layers 1 and 3 of the presubiculum, avoiding layer 2 (Simonnet et al., 2017; Nassar et al., 2018). Labeling was precisely limited to the presubiculum with a sharp reduction of green fluorescence at the posterior border with the parasubiculum, the anterior border with the subiculum and the lateral border with deep layers. Axon terminals in layer 3 were not homogeneously distributed. Patches of higher density were evident in deep layer 3 (Fig. 1G). Along the dorso-ventral axis, ATN axons projected from -2 to -4 mm ventral to Bregma. Fluorescence was not detected in adjacent regions including the Sub, PaS, and DG. ATN axons avoided layer 2 of the PrS, including anterior regions with patches of calbindin positive neurons that project to contralateral PrS (Preston-Ferrer et al. 2016; Fig. 1K).

RSC projections to the presubiculum (Fig. 1H), traced with the fluorescent Chronos-GFP construct, also projected to layers 1 and 3. Unlike ATN axons, they were restricted to dorsal regions of the presubiculum (from -2 to -3 mm ventrally to Bregma on the dorso-ventral axis; Fig. 1H, I, J). RSC axon labeling tended to avoid patches of high-density ATN projections (Fig. 1G, K. Fig. 3). Overall, these data show ATN and RSC afferents innervate overlapping dorsal regions of the PrS, in layer 1 and deep

parts of layer 3. Different spatial patterns of fiber terminations suggest distinct local connectivities.

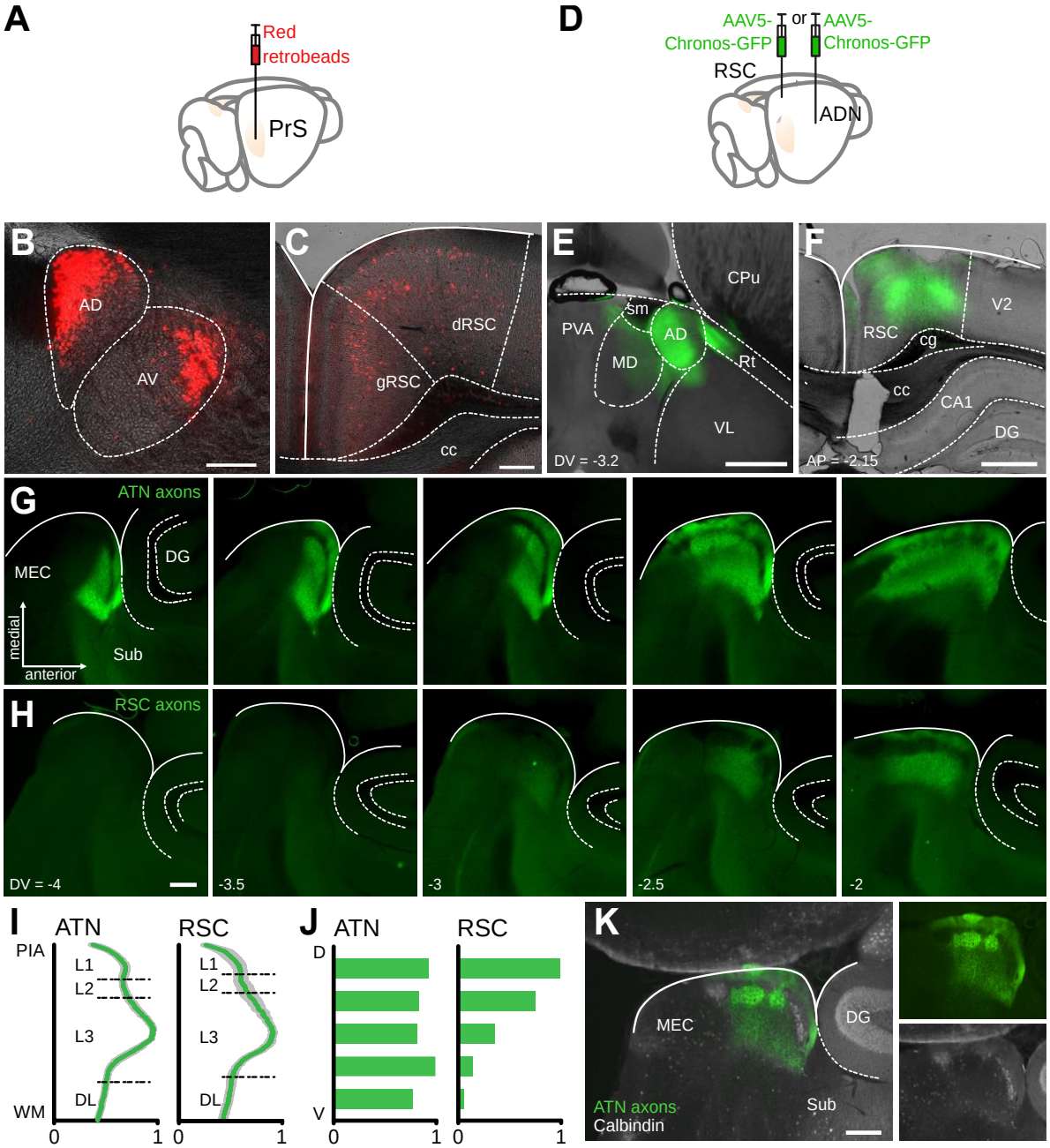

Figure 1. ATN and RSC send strong axonal projections to the superficial layers of dorsal Presubiculum

A, Retrograde labeling of cortical and subcortical regions projecting to the presubiculum (PrS) with retrobeads.

B, Ipsilateral anterodorsal and anteroventral thalamic nuclei are labeled with beads.

C, Ipsilateral granular (gRSC) and dysgranular (dRSC) retrosplenial cortex labeling. Scale bars B, C 200 µm.

D, Anterograde labeling of thalamic and retrosplenial projections to PrS with AAV-Chronos-GFP.

E, F, Injection sites in ATN (E) and RSC (F). AD: anterodorsal thalamic nucleus, AV: anteroventral thalamic nucleus, CA1: field of the hippocampus, cc: corpus callosum, cg: cingulum, CPu: caudate putamen, DG: dentate gyrus, MD: thalamic medial dorsal nucleus, MEC: medial entorhinal cortex, PaS: parasubiculum, PVA: paraventricular thalamic nucleus, anterior, Rt: thalamic reticular nucleus, sm: stria medullaris, Sub: subiculum, VL: thalamic ventrolateral nucleus.

G, H, Five sequential 100-µm horizontal slices of the parahippocampal region show ATN (G) and RSC (H) axons expressing Chronos-GFP (green). Dashed lines show limits of the parahippocampal region to the left and of the

dentate gyrus to the right. Numbers show dorsoventral level with respect to bregma. Scale bars 100 µm.
I, Normalized profiles of fluorescent intensity for ATN and RSC projections to the presubiculum, from white matter (WM) to pia (PIA). Mean (green) ± SEM (grey), n = 8.
J, Ventral (V) to dorsal (D) normalized distribution of ATN and RSC projections to the presubiculum, n = 3 mice.
K, ATN axon labeling (green) is segregated from calbindin labeling (white) in the PrS. Scale bar 100 µm.

Layer 3 neurons are directly excited by both ATN and RSC afferents

We next examined physiological effects of ATN and RSC afferents on PrS pyramidal cells (Rees et al., 2017). Responses to photo-stimulation of the Chronos-GFP construct injected either in the thalamus or in the retrosplenial cortex (Fig. 2A) were recorded in layer 3 neurons (Fig. 2B). These cells had robust regular firing patterns in response to depolarizing current injections (Fig. 2C). Intrinsic properties of layer 3 cells were rather uniform (Table S2) and an unsupervised cluster analysis suggested they formed a single population (Fig. 2D).

Blue light activation of either ATN or RSC axons expressing Chronos-GFP reliably evoked synaptic responses in whole-cell patch-clamp records from layer 3 cells. High intensity stimulation (1 - 3 mW) evoked EPSCs or EPSPs with a probability of 84% (70/83) for ATN fibers and 85% (104/123) for RSC fibers (Fig. 2E). Excitatory postsynaptic currents or potentials evoked by optical stimulation of thalamic and retrosplenial inputs will be referred to as oEPSCs and oEPSPs. Mean oEPSC amplitudes (Fig. 2F) were similar for ATN (-305.0 ± 61.0 pA, n = 24) and RSC fiber stimuli (-305.8 ± 59.1 pA, n = 27). Response latency (Fig. 2G) to ATN axon stimulation was 2.45 ± 0.19 ms (n = 24) and that for RSC axon stimulation was 2.93 ± 0.23 ms (n = 27). The variability in latency of oEPSCs (Supp. Fig. 3A, B) induced by RSC afferent stimuli was 0.35 ± 0.09 ms (n = 27) and that for oEPSCs induced by ATN stimuli was 0.19 ± 0.06 ms (n = 24). These short oEPSC latencies suggest monosynaptic transmission. We confirmed this point by showing that oEPSCs were maintained in presence of TTX (1µM) and 4AP (100µM) (Fig. 2H, n = 2 and 12 for ATN and RSC respectively). EPSCs induced by stimulation of ATN and RSC fibers were reduced in amplitude and decayed more quickly in the presence of the NMDA receptor antagonist APV (50 µM) and were completely abolished by further application of the AMPA receptor antagonist NBQX (1 mM) (Fig. 2I). The shape of oEPSCs induced by light stimulation of ATN and RSC fibers was comparable. Rise times (Supp. Fig. 3C-E) were 1.38 ± 0.15 ms for ATN EPSCs (n = 15) and 1.38 ± 0.08 ms for RSC-mediated EPSCs (n = 15) and mean half-widths were 4.00 ± 1.02 ms for ATN-induced ESPCs (n = 15) and 4.34 ± 1.18 ms for RSC EPSCs (n = 15). The mean time constant (tau decay) for ATN-mediated EPSCs was 3.01 ± 0.21 (n = 15) and for RSC-induced EPSCs 3.17 ± 0.27 (n = 15).

Optical stimulation of ATN and RSC fibers at lower light intensities elicited sub-threshold synaptic events in layer 3 cells. oEPSP amplitude for ATN mediated events was 4.09 ± 1.18 mV (n = 11) and for RSC events it was 4.80 ± 0.84 mV (n = 11). Maximal slopes were 2.93 ± 0.82 mV/ms for ATN-mediated events (n = 11) and 3.02 ± 0.53 mV/ms for RSC EPSPs (n = 11), while time constants were 81.4 ± 11.6 ms for ATN EPSPs (n = 11) and 86.9 ± 11.2 ms for RSC EPSPs (n = 11). Rise times were shorter for subthreshold EPSPs induced by ATN afferents at 3.00 ± 0.24 ms (n = 11) while those for RSC initiated EPSPs were 3.59 ± 0.34 (n = 11, p = 0.042, Wilcoxon test; Supp. Fig. 4A-E). These data show that ATN and RSC axons make monosynaptic, glutamatergic excitatory contacts on layer 3 PrS cells.

The dynamics of responses to repetitive stimulation of layer 3 PrS cells were tested using 20 Hz trains of light stimuli to activate either ATN or RSC afferents. oEPSCs for both inputs followed depressing kinetics. Amplitude decreased for both inputs (Fig. 2J, K), significantly after the fourth pulse

(Friedman's test and Dunn's multiple comparison test). The *10/1* ratio was significantly lower than the paired-pulse ratio (PPR) in both cases (ATN *10/1* 0.56 ± 0.05 vs PPR 0.86 ± 0.05, n = 15, $p < 0.0001$, Wilcoxon test, RSC *10/1* 0.64 ± 0.05 vs PPR 0.83 ± 0.03, n = 15, Wilcoxon test) (Fig 2L). ATN fiber stimulation induced PrS cell firing in current-clamp with a high probability for initial stimuli and lower stable probabilities for later stimuli in the train. Similarly, 20 Hz stimulation of RSC afferents evoked spikes with high probability for initial stimuli and decreasing probabilities for later stimuli (on fourth and 7th-10th pulses, Friedman's and Dunn's multiple comparison tests; Fig. 2M, N). Responses to repeated subthreshold stimuli had similar dynamics (Fig. 2O). Stimulation with lower light intensities (< 1 mW) to initiate sub-threshold oEPSPs elicited different dynamic responses. ATN afferent trains elicited responses with depressing dynamics: the amplitude of the fifth oEPSP was significantly less than the first one (3.18 ± 0.88 vs 5.11 ± 1.64 mV, $p = 0.0185$, Friedman's and Dunn's tests). In contrast, subthreshold 20 Hz stimulation of RSC afferents evoked little or no oEPSP depression (Supp Fig. 4F-H). These data reveal distinct patterns of integration of repetitive activity in glutamatergic ATN and RSC afferents terminating on PrS layer 3 pyramidal cells.

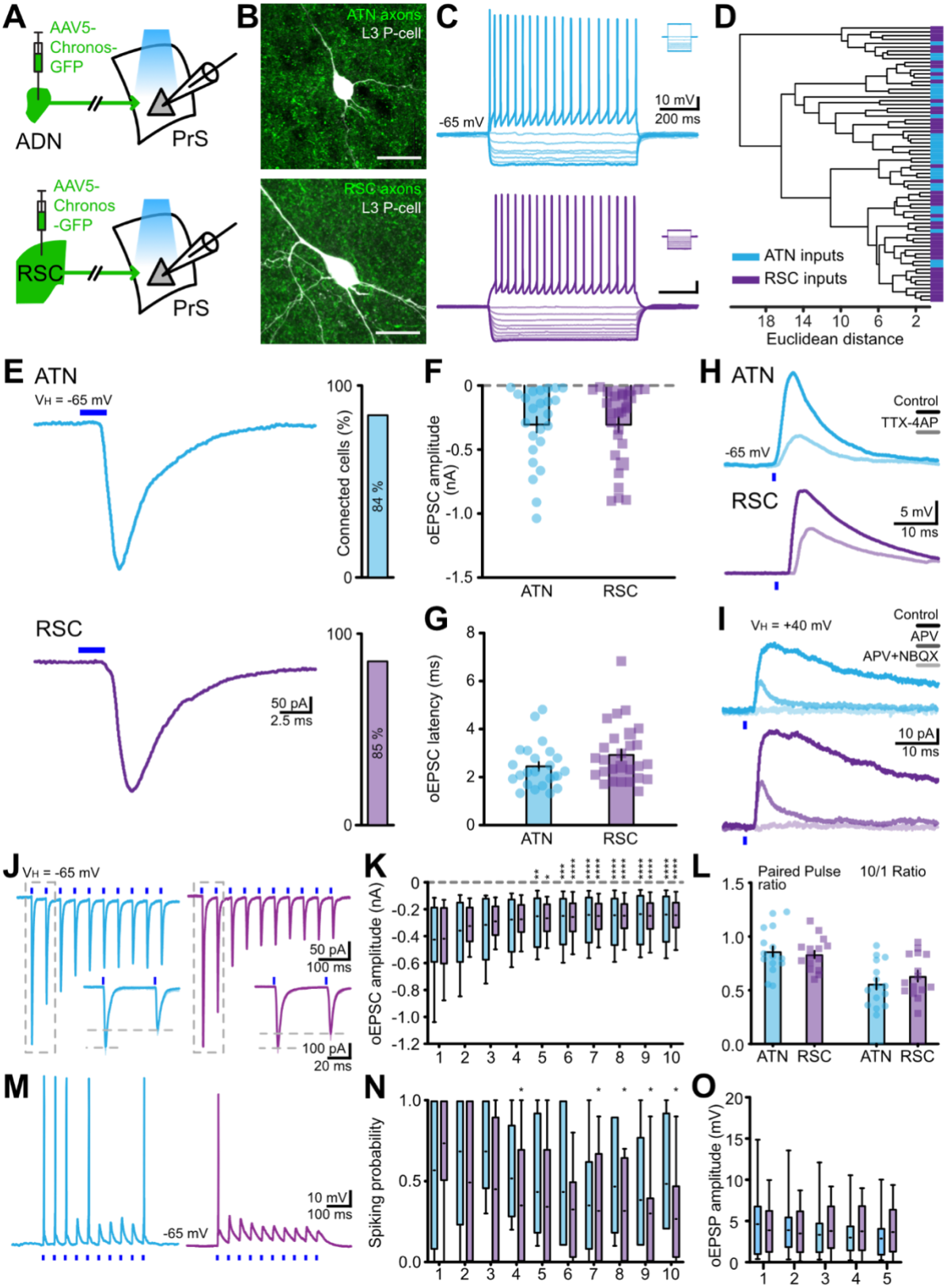

Figure 2. Responses of layer 3 presubicular cells to activation of ATN and RSC fibers.

A, Experimental design. AAV5-Chronos is stereotaxically injected into ATN or RSC

B, Biocytin labeled layer 3 cells (white) and GFP positive axons (green) from the ATN or RSC. Scale bar 10 µm.

C, Firing pattern of two layer 3 cells receiving inputs from the ATN (*cerulean*) and the RSC (*purple*). Insets show current commands.

D, Cluster analysis of physiological parameters for cells tested by stimulating ATN or RSC fibers.

E, Representative EPSCs evoked in layer 3 cells by light stimulation (blue bar) of ATN or RSC inputs. Right, proportion of cells receiving ATN or RSC inputs.
F, Average amplitudes of ATN and RSC induced synaptic currents.
G, Latency of EPSCs evoked by light-stimulation of ATN (n = 24 cells) or RSC fibers (n = 27 cells).
H, EPSPs induced in layer 3 cells (single traces) by stimulating ATN or RSC inputs in absence and presence of 1 µM TTX and 100 µM 4-AP.
I, EPSCs induced by stimulating ATN or RSC fibers in the absence and presence of 100 µM APV and APV + 10 µM NBQX. Holding potential +40 mV.
J, Voltage-clamp responses of layer 3 cells to 20 Hz train stimulations of ATN (*left*) and RSC (*right*) inputs. Insets show EPSCs in response to the first two stimuli.
K, oEPSC amplitudes for 10 ATN or RSC fiber stimuli at 20 Hz. n = 15 neurons. Short middle line, mean; Min to max and quartiles.
L, Paired-pulse ratio (PPR) and 10/1 ratio (ratio between 10th and 1st event amplitudes) for ATN or RSC inputs. Wilcoxon matched-pairs signed rank test: ATN PPR vs 10/1 **** $p < 0.0001$, RSC PPR vs 10/1 *** $p = 0.0001$.
M, Current clamp traces showing action potentials and EPSPs evoked by 10 stimuli at 20 Hz.
N, Spiking probability during trains of 10 stimuli. ATN, n = 6, RSC, n = 12. Full line, median; short line, mean; Min to max and quartiles. In K and N, * $p < 0.05$, ** $p < 0.01$, *** $p < 0.001$, **** $p < 0.0001$ from Friedman's test followed by Dunn's *post-hoc* test.
O, oEPSP amplitudes for trains of 5 stimuli at 20 Hz.

Convergence of ATN and RSC inputs on single layer 3 neurons

Are single layer 3 pyramidal cells innervated by both ATN and RSC afferents? It seemed likely since the probability of connection to a given cell was 84% for ATN fibers and 85% for RSC afferents, and cluster analysis (Fig. 2D) provided no evidence for subpopulations of layer 3 cells (but see Balsamo et al., 2022).

We tested the hypothesis using photostimulation at two different light frequencies to activate ATN and RSC afferents independently. However this approach may be compromised since there is an overlap in the excitation spectra of blue-light activated Chronos (400-600 nm) and red-light activated Chrimson (450-700 nm; Klapoetke et al., 2014). Excitation of Chronos with high intensities of blue light might also excite Chrimson. Stimulating with red light at 630 nm should elicit neurotransmitter release in Chrimson-containing but not Chronos-expressing fibers, which we found was indeed the case (Supp. Fig. 6A). Blue light stimuli at 470 nm and intensities higher than 0.01 mW elicited oEPSPs in layer 3 cells of animals with Chronos-expressing fibers. In contrast, blue light intensities higher than 0.25 mW were needed to induce oEPSPs in different animals with Chrimson-expressing axons (Supp. Fig. 5, 6B). Moreover, the amplitude of these events was smaller in Chrimson-injected than in Chronos-injected mice. Thus, in our experimental conditions, blue light intensities up to 0.25 mW could be used to excite Chronos-positive axons with confidence that Chrimson-expressing fibers would not be stimulated.

We also tested the inverse, red light component of the dual stimulus strategy. Intensities were tested in mice injected either with AAV5-Chronos to label ATN fibers or AAV5-Chrimson to label RSC afferents. The strategy was validated by showing that red light induced oEPSPs in Chrimson-containing, but not Chronos-expressing fibers, while blue light evoked synaptic events in Chronos-, but not Chrimson-expressing fibers (Supp. Fig. 6C-H, Supp. Table 3).

Injection in the same animal of the Chronos construction to the thalamus and that for Chrimson to the retrosplenial cortex let us visualize ATN and RSC afferents to the presubiculum (Fig.

3A, B). Axon terminal fields of ATN and RSC projections were evident in superficial layers of dorsal PrS (cf. Fig. 1). Layer specificities, and labeling inhomogeneities were apparent as were high density ATN patches below layer 2 with no RSC axon innervation (Fig. 3B). Layer 3 pyramidal cells could be innervated by ATN and RSC contacts both with apical dendrites in layer 1 and basilar dendrites of layer 3 (Fig. 3D). We found optical stimulation of ATN and RSC axons, evoked synaptic responses in 14 out of 17 layer 3 pyramidal cells tested (current-clamp and voltage-clamp; Fig. 3E, F).

In order to quantify substrates of these innervations, we counted numbers of labeled ATN or RSC terminals located at less than 1µm from dendrites of biocytin filled layer 3 pyramidal cells (n = 6; Fig. 3G). The distribution of these potential contact sites on dendritic trees of layer 3 neurons was diverse. Some neurons exhibited highly segregated domains receiving either ATN or RSC inputs. For instance, cell 1 had a high proportion of clustered RSC putative synapses on its apical tuft while basilar dendrites were mostly surrounded by potential thalamic terminals. In cell 2, RSC terminals were clustered close to apical dendrites and also together with ATN terminals close to basilar dendrites. In contrast, many ATN terminals were located closer to apical dendrites of cell 3. Segregation of cortical RSC inputs to apical dendrites and thalamic ATN inputs to basal dendrites might favor supralinear EPSP summation. However, afferent terminal distributions differed and we found no clear pattern of linearity scores (cell 1, supralinear (1.39); cell 2, roughly linear (0.91); cell 3, sublinear score (0.69), Fig. 3G, H). Furthermore, we noted certain potential contacts were located with separations less than 20 µm on the same dendrite (Fig. 3I). Such proximity might underly local dendritic computations and supra-linearities such as NMDA-mediated dendritic spikes which are suggested to contribute to non-linear summation of synaptic events (Larkum et al., 1999, 2007, 2009).

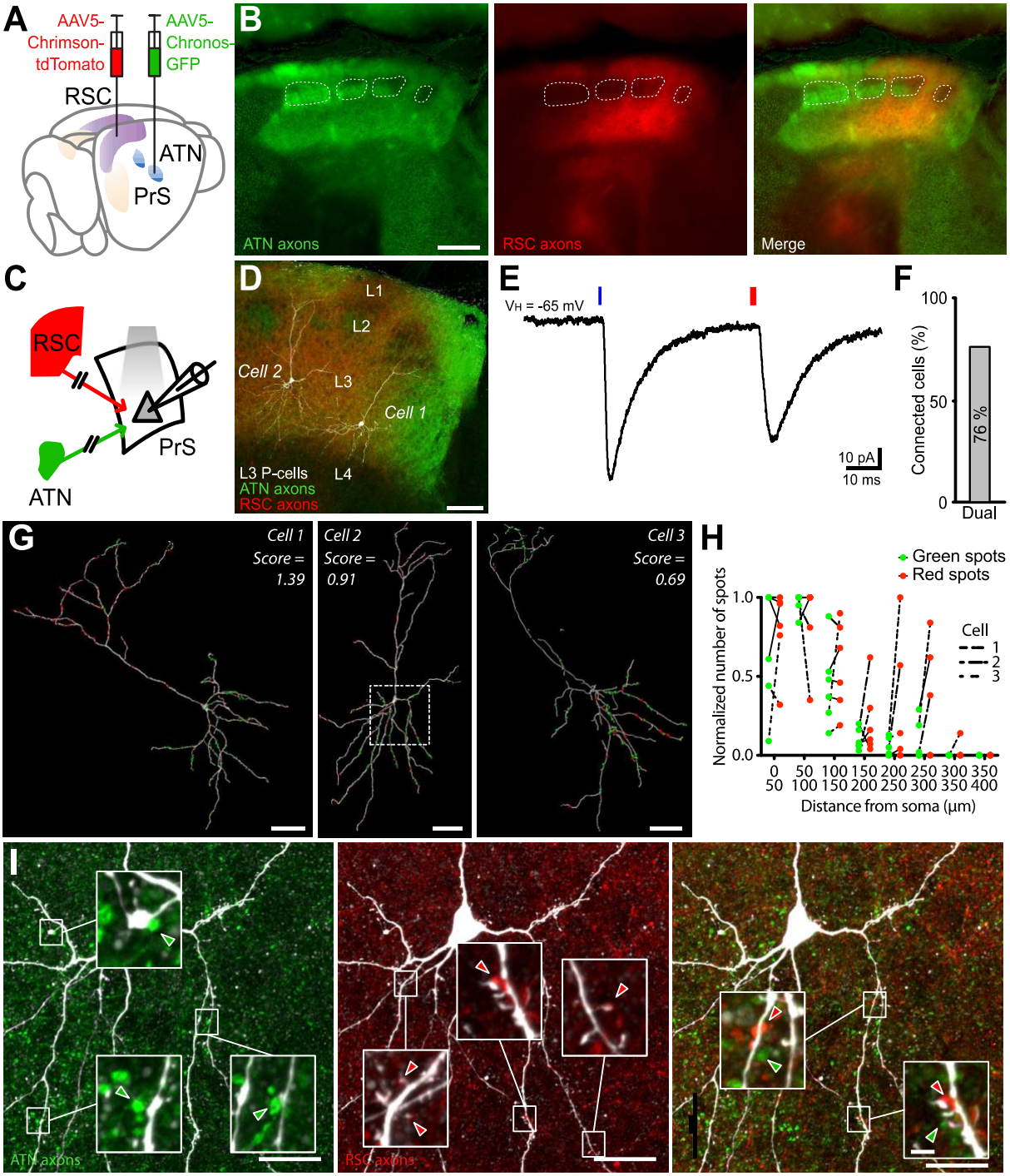

Figure 3. Opsin expressing ATN and RSC axons contact single L3 pyramidal neurons in dorsal presubiculum.

A, Experimental design. AAV5-Chronos-GFP and AAV5-Chrimson-tdTom are injected into ATN and RSC respectively.

B, Axons from ATN (green) and RSC (red) in superficial layers of dorsal presubiculum. RSC fibers avoid patch-like microstructures formed by ATN fibers in upper layer 3. Scale bar, 200 µm.

C, Presubicular layer 3 cells recorded in double injected mice.

D, Two biocytin labeled PrS layer 3 pyramidal cells surrounded by ATN (green) and RSC (red) axons.

E, EPSCs evoked by photostimulation of either ATN (blue light) or RSC fibers (red light).

F, 13/17 (76%) of layer 3 pyramidal neurons receive synaptic inputs from both ATN and RSC afferents.

G, Distributions of putative ATN (green) and RSC (red) synapses on the dendrites of three layer 3 neurons. The linearity score is indicated. Scale bar 50 µm. The dotted square area on Cell 2 is enlarged in panel I.

H, Normalized number of green and red spots for 6 neurons as a function of the distance from soma. Paired values are indicated by dotted lines for the 3 cells in G.
I, Examples of ATN-labeled (left), RSC-labeled (middle) and both (right) synapses closely apposed to dendrites of a biocytin-filled layer 3 pyramidal cell. Scale bar 20 µm. Insets show enlarged views. Scale bar 2µm.

Supralinear subthreshold integration and amplification of ATN and RSC excitatory postsynaptic potentials

We explored interactions between excitatory inputs to layer 3 neurons by stimulating ATN and RSC axons separately with blue or red light. Excitatory synaptic potentials evoked by ATN or RSC axon stimulation, were compared to responses elicited when both sets of axons were activated at short time intervals (dual; Fig. 4A). The mean amplitude of dual oESPs (synchronous light onset, Fig. 4A-C) was significantly larger than calculated summed amplitudes of single oEPSPs (n = 11 cells, dual/summed amplitude 2.06 ± 0.55 mV, p = 0.0068, Wilcoxon test). Charge transfer, quantified as the surface under the dual oEPSP, was greater than the summed values for single oEPSPs (Dual/summed surface 2.21 ± 0.54 mV.s, n = 11, p = 0.0098, Wilcoxon test). These mean values cover variability between individual neurons. Summation of responses to ATN and RSC axon stimuli was supralinear in 7 out of 11 cells tested, linear for 3 cells and sublinear for 1 cell.

Dynamic responses to repetitive stimulations were also transformed by dual photostimulation. Amplitudes of 5 dual oEPSPs elicited at 20 Hz were higher than for a linear summation (Amplitude in mV – Summed vs. Dual: Stim 1, 7.7 ± 1.9 vs. 11.1 ± 1.9; Stim 2, 6.7 ± 1.6 vs. 9.5 ± 1.5; Stim 3, 6.5 ± 1.4 vs. 9.5 ± 1.5; Stim 4, 6.1 ± 1.3 vs. 9.2 ± 1.5; Stim 5, 5.9 ± 1.3 vs. 8.6 ± 1.4, p = 0.0117, Two-way ANOVA; Fig. 4E) and charge transfer, quantified as the surface under the 5 oEPSPs, also typically summed supralinearly (20 Hz, Surface in mV.s – Summed vs. Dual: Stim 1, 136.9 ± 30.6 vs. 221.2 ± 41.5; Stim 2, 143.3 ± 25.7 vs. 242 ± 43.9; Stim 3, 147.3 ± 22.5 vs. 259.2 ± 44; Stim 4, 145.1 ± 22 vs. 263.5 ± 49.2; Stim 5, 145.6 ± 23.2 vs. 258.7 ± 45.2, p = 0.0128, Two-way ANOVA; Fig. 4F). Trains of dual ATN and RSC fiber stimulations also showed increased oEPSP integrals, compared to the stimulation of either one set of fibers alone, indicating stronger excitation over time (Fig. 4E, F). Taken together, these data show supralinear summation of ATN and RSC inputs in most single layer 3 pyramidal cells, and also a facilitation of dynamic responses to repetitive inputs at 20 Hz.

We next asked how efficiently action potentials were induced by combined ATN and RSC inputs. Firing probability of layer 3 cells was higher for dual than for single input stimulation at a membrane potential of -65 mV (ATN 0.008 vs Dual 0.268, n = 5, p = 0.0216, RSC 0.024 vs Dual 0.268, n = 5, p = 0.1195, Friedman's and Dunn's tests) and higher still at -55 mV (Fig. 4G, H). Firing was induced over a narrow window of time delays between stimulation of the two inputs (Fig. 4I, J). It occurred for delays of -2 to +5 ms (RSC preceding ATN stimulus) reaching a maximum at a delay of +1 ms.

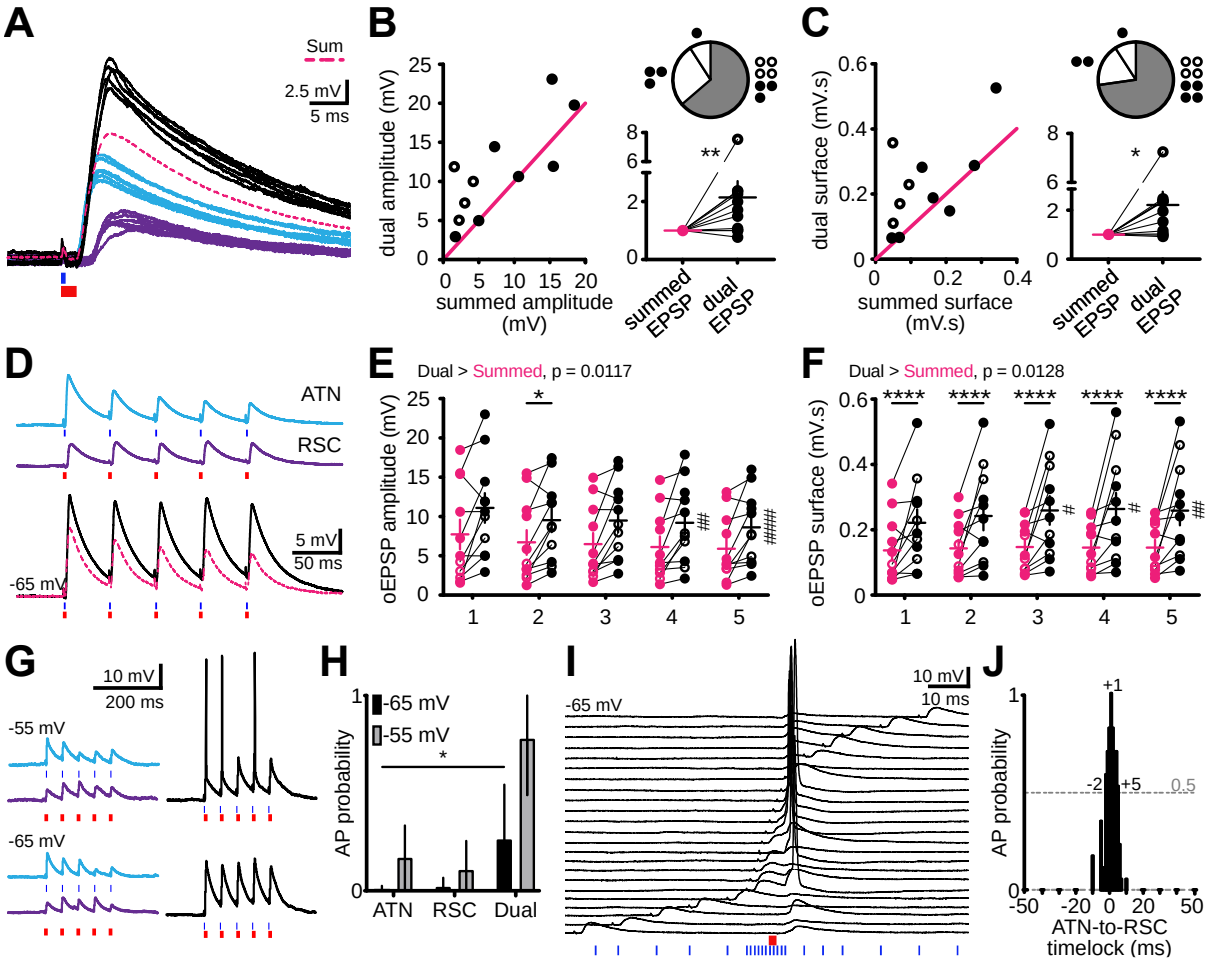

Figure 4. Supralinear subthreshold summation and action potential firing elicited in layer 3 neurons by near-coincident stimulation of ATN and RSC axons.

A, Excitatory postsynaptic responses in layer 3 neurons to stimulation of either ATN axons (blue light, cerulean traces), RSC axons (red light, purple traces) or both (blue and red light, black traces). The arithmetical sum of averaged oEPSPs evoked by stimulation of either ATN or RSC axons is indicated in pink (broken line). Records from cell 1, Fig 3D.

B, C, Amplitude (B) and integral (C) of dual oEPSPs plotted as a function of the calculated average sum of ATN and RSC oEPSPs (*left*). Each circle is a recorded L3 cell (n=11), Pink line (± 10%) indicates linearity. Pie charts summarize the number of tested neurons with supralinear (grey), linear (pink) or sublinear (white) summation. oEPSPs normalized to linear sum (*bottom right*). Solid circle, Chronos in ATN/Chrimson in RSC, empty circle, Chronos in RSC/Chrimson in ATN. * $p < 0.05$, ** $p < 0.01$, from Wilcoxon test.

D, oEPSPs induced by 20 Hz trains of ATN (light blue), RSC (purple) or dual (black) stimuli. The calculated average sum of oEPSPs evoked by separate ATN and RSC photostimulation is indicated in pink (broken line).

E, F, Amplitude (E) and integral (F) of dual subthreshold oEPSPs compared to the calculated average sum of ATN and RSC oEPSPs, for each postsynaptic response to a train of 5 stimulations at 20 Hz. Two-way ANOVA statistical p value is indicated on top of the graph. * $p < 0.05$, **** $p < 0.0001$, Šidák's multiple comparison test. # $p < 0.05$, ## $p < 0.01$, Friedman's and *post-hoc* Dunn's test.

G, Excitatory postsynaptic responses to photostimulation of ATN (blue light, cerulean traces) or RSC axons (red light, purple traces) or both (blue and red light, black traces) at resting membrane potential (-65 mV) and at a depolarized holding potential (-55 mV). Synaptic excitation led to cell firing on some dual ATN and RSC stimuli at the depolarized holding potential.

H, Action potential (AP) probability for either or both stimuli at -65 and -55 mV.

I, Responses to stimulating ATN fibers (blue light) and RSC fibers (red light) with varying time delays from -40 to +40 ms.
J, AP firing probability is maximal for short delays between -2 to +5 ms (RSC preceding ATN).

Supralinear summed responses of excitatory synaptic events may be mediated via the activation of NMDA receptors or voltage dependent intrinsic currents that amplify EPSPs (Fricker and Miles, 2000), especially if synaptic inhibition is reduced. We assessed these mechanisms in records made from layer 3 pyramidal neurons using a Cesium-based internal solution to favor cationic amplifying currents, and also containing QX314 to suppress action potentials (Fig. 5). In 3 cells photostimulation of ATN fibers evoked oEPSPs of amplitude 10.9 ± 2.0 mV and RSC fiber stimulation induced events of 13.7 ± 2.5 mV. The response dynamics to 5 light pulses at 20 Hz were moderately facilitating (2nd vs 1st amplitude ratio: ATN 1.39, RSC 1.17; 5th vs 1st: ATN 1.18, RSC 1.20; n = 3). Coincident activation of ATN and RSC afferents induced supralinear oEPSP summation. Furthermore, repetitive stimulation generated large all-or-none depolarizations on the second or third stimulus at 20 Hz (2nd vs 1st amplitude ratio: 1.52; 5th vs 1st: 2.90; n = 3 cells, Fig. 5A). It may be mediated by VGCC or a QX-314 resistant Na+ inward current (Fricker et al., 2009). This component appeared with higher probability and shorter latency in the presence of $GABA_A$ receptor blocker gabazine (Fig. 5B). The NMDA receptor antagonist APV largely abolished the dual EPSP amplification initially (Fig. 5C, black trace; 2nd vs 1st integral ratio: 1.22; 5th vs 1st: 1.32), although amplification was partially restored by increasing RSC stimulus intensity (pale pink trace). NMDA receptor activation thus assists depolarization towards the threshold of a voltage-dependent process contributing to supra-linear EPSP summation, but is not the only charge carrier involved.

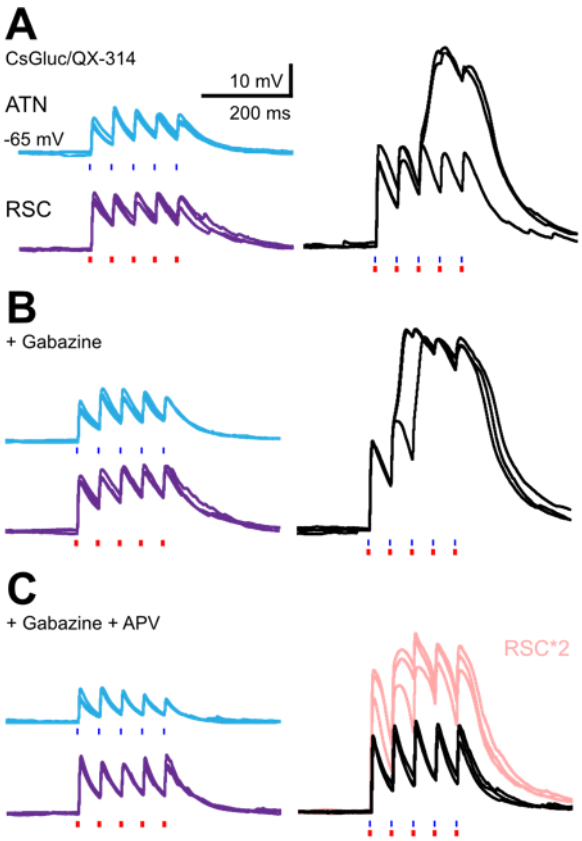

Figure 5. All-or-none postsynaptic events induced by repetitive stimuli in layer 3 pyramidal neurons.
A, Responses of layer 3 pyramidal neurons to stimulation of ATN axons (blue light, cerulean traces), RSC axons (red light, purple traces) and both (blue and red light, black traces). Recordings were carried out at resting membrane potential (-65 mV). Recording pipette contained a cesium based internal solution and the Na^+ channel blocker QX-314. A large all–or-none EPSP amplification occurred on the third dual stimulus of a 20 Hz train.
B, In the presence of the $GABA_A$ receptor antagonist gabazine (10 µM), EPSP amplification appears earlier in the train.
C, In the additional presence of the NMDA receptor antagonist APV (100 µM), dual EPSP amplification was abolished (black trace). It was partially restored by increasing RSC stimulation intensity (pale pink traces).

Recruitment of presubicular layer 4 neurons by ATN and RSC afferents

Presubicular layer 4 neurons are intrinsic bursting pyramidal neurons that project to the lateral mammillary nucleus (Huang et al., 2017). This pathway is critical for the coordinated stable landmark control of HD cells in the thalamus and throughout the HD cell circuit (Yoder et al., 2015). To investigate the input connectivity of layer 4 principal cells, we recorded responses of these neurons to stimulation of ATN and RSC afferents.

Layer 4 neurons labeled by retrograde tracers injected in the lateral mammillary nucleus were located in the *lamina dissecans* of the presubiculum, below layer 3, where thalamic axons ramify (Fig. 6A-D). The apical dendrites of layer 4 pyramidal neurons extended towards presubicular layer 1 as previously described (Huang et al., 2017), but tended to circumvent layer 3 and avoid thalamic afferents, by swerving towards the subiculum. Apical dendrites of some neurons crossed layer 3 obliquely, while others avoided thalamic afferents in layer 3 (Fig. 6C, D, Supp. Fig. 7, 8).

Layer 4 neurons had a more depolarized resting membrane potential, lower input resistance and time constant than layer 3 neurons (Supp. Fig. 9 compares active and passive properties). A characteristic voltage sag in responses to hyperpolarizing steps, indicated the presence of an I_h current. Layer 4 neurons discharged bursts of two or three action potentials at the onset of a depolarizing step current injection and also after the offset of hyperpolarizing steps (Fig. 6E). These bursts were abolished by the T-type Ca^{2+} channel blocker TTA-P2 (Fig. 6F).

We next recorded responses of layer 4 neurons to optical activation of ATN or RSC afferents together with effects of the same stimuli on layer 3 pyramidal cells (Fig. 6G). Overall, latencies of oEPSCs in layer 4 neurons were longer than for layer 3 (ATN layer 4, 6.2 ± 0.6 ms, n = 8, vs. layer 3, 2.4 ± 0.2 ms, n = 24; RSC layer 4, 5.6 ± 0.4 ms, n = 9, vs. layer 3, 2.9 ± 0.2 ms, n = 27; Fig. 6H), indicating possible polysynaptic excitation of layer 4 neurons. Bath application of TTX-4AP did not abolish oEPSPs entirely, leaving a low amplitude component with short, potentially monosynaptic latencies (latency ATN 3.9 ± 0.6 ms, RSC 2.9 ± 0.2 ms, n = 5; Fig. 6I).

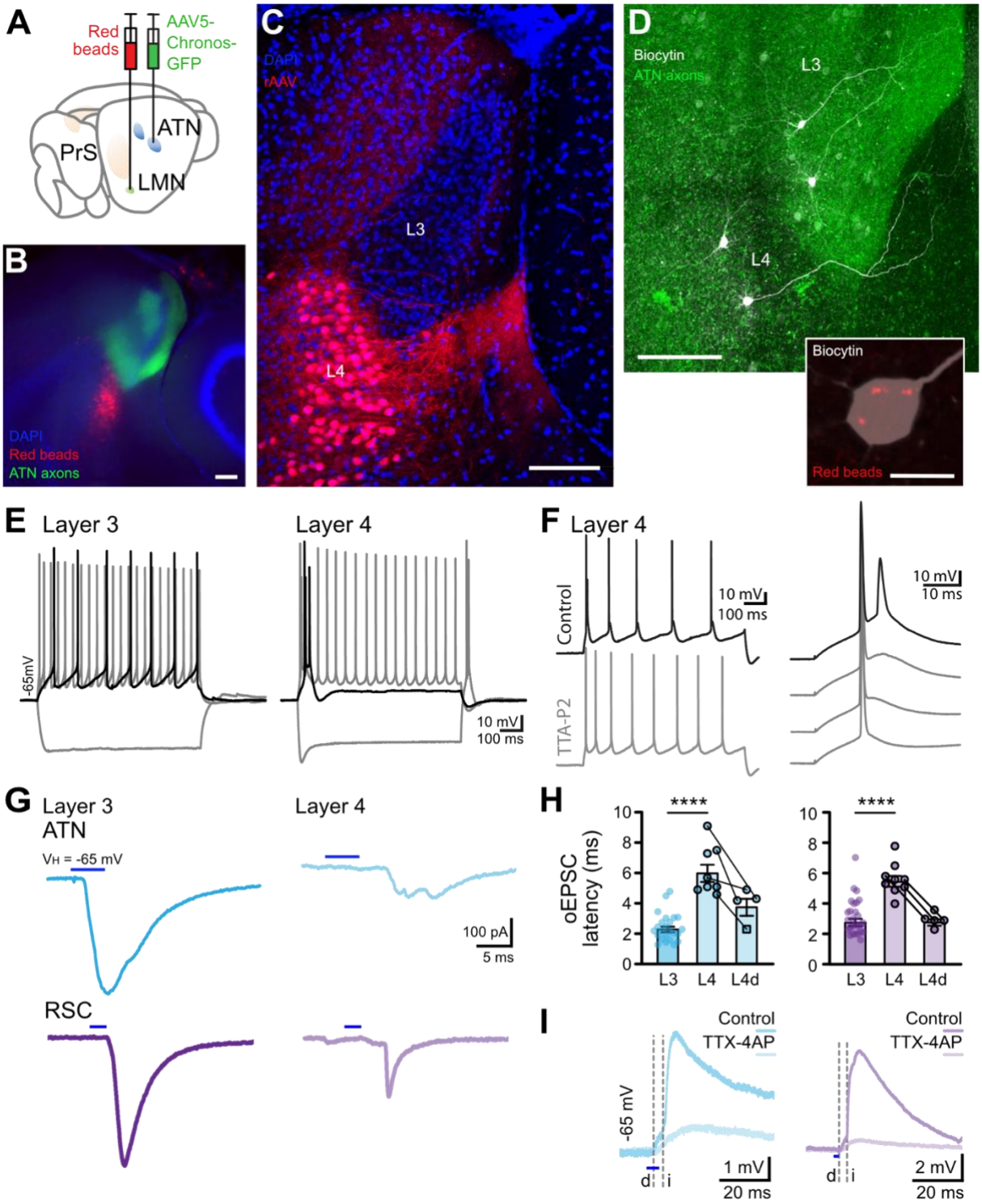

Figure 6. LMN-projecting layer 4 bursting neurons are indirectly recruited by thalamic and retrosplenial inputs.

A, AAV-Chronos-GFP was injected in the anterior thalamus and red retrobeads in the LMN.

B, Thalamic axons (*green*) targeting superficial layers 1 and 3 of presubiculum. Retrobeads label layer 4 cells projecting to the LMN.

C, Retrograde labeling by AAV2retro. Apical dendrites of layer 4 pyramidal neurons avoid layer 3 where thalamic axons ramify.

D, Two layer 3 and two L4 neurons filled with biocytin (white), surrounded by GFP thalamic afferents (green). Scale bar 100 µm. Inset, retrobeads (red) in the soma of a LMN-projecting layer 4 neuron. Scale bar 10 µm.

E, Representative firing patterns of layer 3 and layer 4 neurons. Grey traces represent responses to injection of

hyperpolarizing and depolarizing current pulses. Black trace shows the neuronal response at rheobase.
F, Responses of a layer 4 neuron to depolarizing current injection in control conditions and in presence of TTA-P2 (1 µM), a blocker of T-type Ca^{2+} channels. At left, evolution of the suppression of burst firing by TTA-P2.
G. Voltage-clamp responses of layer 3 and layer 4 pyramidal cells to stimulation of ATN or RSC inputs.
H, oEPSC latency for layer 3 and layer 4 cells for ATN or RSC inputs. Same cells are indicated by connecting line.
I, Current-clamp responses to stimulation of ATN inputs in control conditions and in presence of TTX-4AP. Dashed lines indicate the timing of monosynaptic (d, direct) and disynaptic (i, indirect) components of the response.

Comparison of the timing of synaptic events and firing (Fig 7A-C) showed that oEPSP onset in a layer 4 neuron occurred after firing in the layer 3 neuron, for either ATN (4/5) or RSC (1/1) afferent stimuli. Depolarization of the layer 3 cell via the patch pipette, initiated firing, but EPSPs were not elicited in any simultaneously recorded layer 4 neuron (n = 0 out of 6 cell pairs tested). These data suggest that excitation of layer 3 cells by ATN and RSC afferents is transmitted to layer 4 neurons, even in the absence of direct evidence for mono-synaptic coupling between cell pairs.

In records from pairs of layer 3 and 4 neurons (n = 3; Fig. 7D-H) layer 3 cells responded with precisely timed action potentials to low intensity stimulation of ATN afferents, while only very small oEPSPs were initiated in layer 4 neurons. Increasing the excitatory drive by stimulating RSC afferents elicited larger oEPSPs more reliably in layer 4 neurons. Higher intensity stimulation of both ATN and RSC axons, could evoke bursts of action potentials, with the activation of an underlying Ca^{2+} current in layer 4 cells (Fig. 7E). We hypothesize that increasing the activity of layer 3 neurons by strong (and non-specific) stimulation of ATN and RSC afferents is needed to induce discharges in layer 4 cells. We should also note that strong photostimulation of a single set of afferent fibers could initiate discharges in layer 4 pyramidal cells, as was shown in records from mice where only one afferent brain area, ATN or RSC, expressed an opsin (Supp. Fig. 10).

Overall, it seems probable that layer 3 neurons relay activity projected by ATN and RSC inputs onto layer 4 pyramidal neurons. However, evidence on this point could be improved. In dual records, we did not detect functional synapses between layer 3 and layer 4 neurons (n = 9). Anatomically, putative synaptic contacts between filled axons of layer 3 and dendrites of layer 4 cells, were not evident (n = 5 filled layer 4 cells). On the other hand, we did find a possible synaptic connection between two neighboring L4 neurons (Fig 7F, G), with a close apposition between axon and dendrite. Recurrent excitation may promote bursting in layer 4 neurons, and NMDA receptor related EPSP amplification favors burst firing (Fig. 7H).

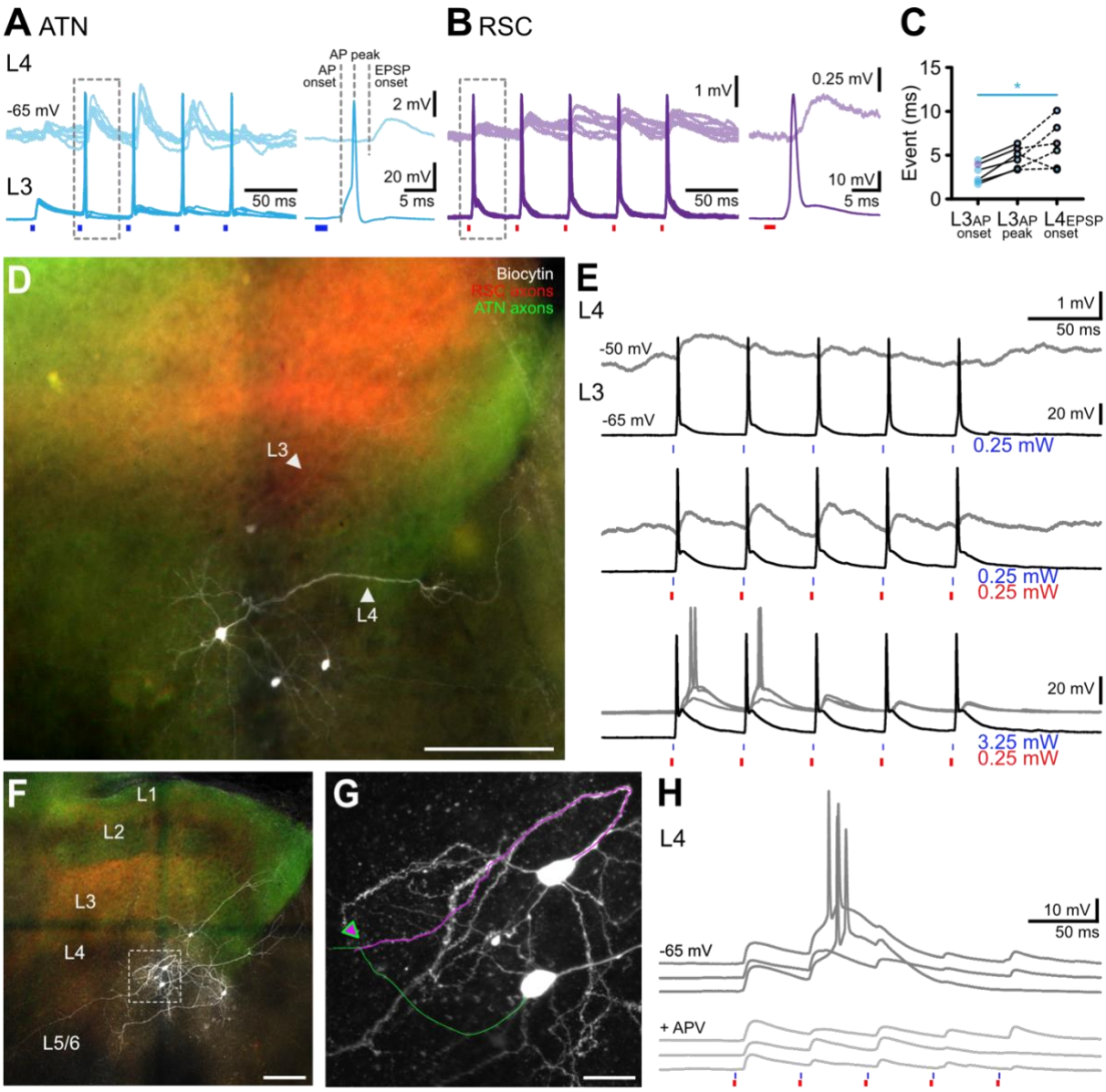

Figure 7. Transsynaptic activation of LMN projecting neurons in layer 4.

A, Simultaneous records of layer 3 (lower) and 4 (upper) neurons during photostimulation of ATN afferents. EPSP onset is delayed in L4 neurons. Right panel is a close-up view of the area in the square.

B, Simultaneous recording of layer 3 and 4 neurons during photostimulation of RSC afferents. As in A, L4 neurons responded with a delay. Right panel is a close-up view of the area in the square.

C, Latencies of synaptic activation indicated by the dotted lines in A, B (ATN stimulation, n = 4 cells; RSC stimulation, n = 1). Full line indicates onset and peak latencies from single layer 3 neurons (n = 5). Dotted lines link to the latencies in simultaneously recorded layer 4 neurons. $p < 0.05$, Kruskal-Wallis multiple comparison test.

D, Biocytin labeled layer 3 and 4 neurons surrounded by thalamic (*green*) and retrosplenial (*red*) axons. Layer 4 apical dendrite crosses layer 3 for a short distance before arborizing outside of ATN targeted area, towards the subiculum. Scale bar, 100µm.

E, Simultaneous records from layer 4 and layer 3 cells to ATN input stimulation (*low amplitude blue*), ATN and RSC (*blue and red, light intensities compatible with independent photostimulation*) or non-specific ATN and RSC (*high amplitude blue and red*) in a Chronos/ATN - Chrimson/RSC double injected mouse.

F, Same configuration as in D. Dotted square is enlarged in G. Scale bar, 100µm.

G, Enlarged confocal image showing a potential synaptic contact between two layer 4 neurons. Pink, the apical dendrite of this L4 neuron makes a U-turn, away from layer 3, where the thalamic axons ramify. Green, axon of

a neighboring L4 neuron. Its apical dendrite extends toward L3 initially, then leaves the thalamo-recipient L3 towards the subiculum at the right. Scale bar 20µm
H, Bursts of action potentials evoked by dual stimulation of ATN and RSC afferents were abolished by the NMDA receptor antagonist APV.

Discussion

Understanding the anchoring of HD signals with visual landmarks provides a useful framework to ask how external information is integrated to revise and improve brain representations. Here we show that thalamic ATN afferents signaling HD data and cortical RSC projections that carry visual landmark information converge on layer 3 pyramidal cells of the dorsal presubiculum. Independent optogenetic stimulation of these two glutamatergic afferents in slices was used to define mechanisms of their integration in the presubiculum. Most layer 3 cells were innervated by both ATN and RSC fibers, sometimes close on the same dendritic branches, sometimes on different dendrites. Nearly coincident EPSPs (2-5 ms) induced independently by ATN and RSC afferents, evoked non-linear membrane responses to trigger layer 3 cell firing, transmitted to the MEC. In a second processing step, layer 3 neurons also excite layer 4 pyramidal cells which receive little direct ATN and RSC innervation. These burst firing neurons, project a distinct, di-synaptically mediated, visually-updated HD signal to the LMN. Our data thus suggest that the presubiculum integrates HD and landmark signals producing two distinct output signals which are transmitted to different regions.

Anatomical convergence of ATN and RSC projections in the dorsal Presubiculum

Retrograde tracing in this study confirmed strong projections to the presubiculum from the ATN and the RSC to the presubiculum (Fig. 1). Anterior thalamic fibers (Van Groen et Wyss 1990c; 1990a; 1990b; 1992; Shibata et Honda 2012; Vogt et Miller 1983) ramify in and delimit the anatomical borders of the presubiculum (Liu et al., 2021; Simonnet et al., 2017). HD signals from HD cells of the anterior thalamus project to the presubiculum (Goodridge and Taube, 1997) where they form synapses directly with layer 3 pyramidal cells (Nassar et al., 2018). The retrosplenial cortex was the most strongly labeled cortical region innervating the presubiculum. We detected retrogradely transported beads in cells of layers 2 and 5 of dysgranular RSC, and layer 5 of the granular RSC across its antero-posterior axis (Sugar and Witter, 2016).
We examined the anatomy and physiology of these two afferent systems to ask how visual landmark signals from the RSC are combined with HD signals relayed via the ATN. Anterograde fiber tracing, with an AAV5 construct expressing Chronos-GFP, confirmed that axons from both regions project to superficial layers of the dorsal presubiculum. No RSC projections were found in ventral PrS for injections in rostral RSC, as previously noted (Jones and Witter 2007; Kononenko and Witter 2012). Both RSC and ATN innervated superficial presubicular layers 1 and 3, while sparing layer 2 containing somata of calbindin positive neurons (Fig. 1K and cf. Balsamo et al. 2022). We detected microzones containing a high density of ATN-positive fibers, but no RSC fibers, in upper layer 3.

Pathway specific functional connectivity onto PrS layer 3 neurons.

Photostimulation of GFP-Chronos expressing axons let us compare synaptic events initiated in layer 3 pyramidal cells by fibers from the ATN or the RSC in dorsal presubiculum slices (Fig. 2). Both ATN and RSC afferents formed mono-synaptic glutamatergic connections with components mediated by NMDA and AMPA receptors. The amplitudes of synaptic currents varied, with an overall similar amplitude distribution for ATN and RSC stimulation. This may be due to variable expression levels (Hooks et al. 2015), or may imply variations in coupling weights across cells. ATN and RSC fiber mediated EPSCs depressed during repetitive activation at 20 Hz. EPSPs induced firing early during repetitive stimulation. RSC inputs tended to produce more sustained EPSP dynamics and slower rise times than ATN afferents for low intensity stimulation. ATN synapses with presubicular pyramidal cells resemble those made by thalamic afferents in the somatosensory cortex - high release with depressing dynamics, (Gil et al., 1999) possibly due to presynaptic expression of VGLut2 (Liu et al., 2021).

Dual wavelength optogenetic stimulation was used for independent activation of intermingled afferents expressing blue-light sensitive Chronos in ATN fibers and red-shifted Chrimson in RSC fibers (Klapoetke et al., 2014). Precautions were taken to avoid cross-stimulation since all channelrhodopsin variants are somewhat sensitive to blue light. With the fast, sensitive opsin Chronos expressed in ATN fibers, synaptic events were induced by very short (0.5 ms), low intensity, 0.25 mW, stimuli. For RSC fibers expressing Chrimson, using light stimuli of duration 2 ms, adjusting intensity up to 2 mW initiated synaptic events of comparable amplitude. Calibration experiments (Supp Fig. 6) provided strong evidence for the independence of responses. While Chrimson has slower dynamics than Chronos (Klapoetke et al., 2014), synaptic events induced by stimulating either opsin were similar, as we showed by swapping the two opsin variants injected in ATN and RSC fibers respectively (Fig. 4).

This dual opsin approach permitted independent stimulation with blue and red light pulses. Most (76%) recorded layer 3 neurons generated synaptic events in response to stimulation of both ATN and RSC fibers providing a substrate for integration of landmark information from the RSC with thalamic HD signals. Layer 3 cell firing was most effectively triggered by nearly coincident inputs (-2 to +5 ms separation, Fig. 4I, J). This is of interest since HD representations in the AD and RSC are highly coherent (Fallahnezhad et al., 2023), with short intervals between spikes in these two regions (< 5ms; van der Goes et al. 2022). Converging inputs from thalamic and retrosplenial axons can therefore excite common postsynaptic presubicular layer 3 neurons with very short delays, such that coincidence detection by these cells will tend to enhance HD signals transmitted to the MEC. Response dynamics to combined stimulation of both inputs at 20 Hz were maintained or facilitating, in contrast to the depressing dynamics of repetitive stimulation of one set of afferent fibers. Combined and temporally precise inputs from ATN and RSC may thus help maintain HD signaling during immobility.

Nonlinear signal integration in layer 3 thalamo-recipient neurons

Convergence of ATN and RSC axons onto single layer 3 pyramidal cells provides the anatomical basis of synaptic integration. Putative synaptic contacts from both afferent fiber systems were found on the basal dendrites of pyramidal cells (Fig. 3), sometimes on the same branch. Photostimulation centered on the soma of recorded neurons predominantly activated synapses on basal dendrites. Supralinear summation could result from local spike-generating mechanisms if the activated synapses were located on a same dendritic branch (Poirazi and Papoutsi, 2020; Polsky et al., 2004). Clustered synapses could also guide the formation of new spines and synapses during integration of landmark information in the HD signal. Learning might bind new inputs into functional synaptic clusters (Hedrick et al., 2022). Our small sample of layer 3 pyramidal cells suggest that both ATN and RSC axons target basal dendrites, and more RSC than ATN axons contact apical dendrites (Fig. 3). Tests on the effects of

precise, near coincident activation of basal and apical synapses could be revealing but were not technically possible in this study. Distinct dendritic inputs to layer 3 cells may improve spatial perception (Takahashi et al., 2016) enhancing HD signal quality by integration with landmark information.

Our data show that EPSPs elicited by nearly coincident ATN and RSC inputs which exceed a threshold are amplified by NMDA receptor activation and voltage gated inward dendritic currents (Fig. 5; Fricker et al. 2009). EPSP amplification is facilitated by a reduction in synaptic inhibition (Fig. 5), indicating that disinhibition may be permissive for supralinearity and gate firing by dynamic modulation of the balance between inhibition and excitation (Milstein et al., 2015). VIP expressing interneurons, which are excited by cholinergic modulation could provide such disinhibition of the presubicular microcircuit (Porter et al., 1999; Slomianka and Geneser, 1991). A 'when-to-learn' signal for HD updating in the presubiculum might function analogously to the promotion by dopamine of associations between sensory cues and head direction cells in the fly compass neurons (Fisher et al., 2022). It is however unclear whether LTP type learning takes place in the mammalian head direction circuit. Presubicular layer 3 cells do not express the GluR1 subunit of AMPA receptors (Martin et al 1993; Ishihara et al., 2016) that is critical for LTP expression (Boehm et al., 2006). The absence of GluR1 might indicate that the thalamo-presubicular synapses in layer 3 function without classical long-term plasticity.

Layer 3 pyramidal cells may be described as multi-compartmental computational devices (Häusser et Mel 2003; Mel 1993; Poirazi, Brannon, et Mel 2003; Spruston 2008) which integrate HD and landmark information. ATN axons drive presubicular HD neurons (Peyrache et al. 2015) and RSC mixed selectivity neurons contribute visual landmark information and allocentric spatial references (Jacob et al. 2017; Mitchell et al. 2018; Vann, Aggleton, et Maguire 2009). NMDA mediated dendritic spikes enhance tuning selectivity in visual cortex (Smith et al. 2013; Wilson et al. 2016) and barrel cortex (Lavzin et al. 2012). Dendritic events in Layer 3 PrS cells may enable binding of visual landmarks with HD tuning. It is tempting to speculate that nonlinear synaptic integration and inhibitory gating may be involved in flexibly updating the allocentric direction of HD cells based on the integration of visual landmark information to the current HD signal. In the primary sensory cortex, nonlinearities act to increase perceptual threshold of sensory information (Takahashi et al. 2016; 2020). The attractor network in the PrS could thus be either stabilized or flexibly reset to external spatial cues.

Functional significance of two-layer processing preceding projection to LMN

Burst-firing layer 4 PrS cells project a distinct version of HD-landmark signals to the LMN. The dendrites of these LMN projecting neurons overlap little with direct ATN and RSC inputs granting partial isolation from direct excitation, and permitting a second level of integration of information from layer 3 neurons. Layer 3 axons may innervate layer 4 neurons basal dendrites, which may be driven to fire by sufficiently strong excitatory inputs from layer 3.

There are advantages to segregating the integration of converging input signals from the updating signal across layers. This separation permits both a fast transmission of an integrated signal to the medial entorhinal cortex, and transmission of a slower integrated signal mediated by burst firing to upstream HD circuit elements. The synaptic threshold implicit in this two-stage system permits a gated, conditional updating. Functionally layer 4 neurons are uniquely positioned to update the HD signal in the LMN with visual landmark information. These cellular and synaptic circuit data support and expand the findings of Yoder et al. (2015). They clarify how the thalamic HD signal integrated with

visual landmark information is relayed to the grid cell system in the medial entorhinal cortex and to the lateral mammillary nuclei.

Limitations

Burst firing may play a role for learning in hierarchical circuits (Naud et al., 2023; Payeur et al., 2021). In the HD circuit, visual landmark information contained in bursts might reset or anchor the HD attractor in the LMN and beyond. The effects of burst firing signals transmitted to the LMN remain to be assessed. Potentially HD signals may be updated with visual signals at several sites including the PrS, but this region uniquely provides a feed-back projection to the lateral mammillary nucleus. Further work on layer 3 to layer 4 transmission is warranted, and the link to spatial perception and behavioural updating needs to be strengthened.

Acknowledgements

This work is supported by the Centre National de la Recherche Scientifique and the Université Paris Cité. DF received funding from the Agence Nationale de la Recherche (ANR-DFG Program, ANR-18-CE92-0051 BURST), from the ERA-NET NEURON Program (ANR-20-NEUR-0005 VELOSO), and the FLAG-ERA HBP Program (ANR-21-HBPR-0002 VIPattract). This work has benefited from support by the BioMedTech Facilities at Université Paris Cité (Institut National de la Santé et de la Recherche Médicale Unité S36/Unité Mixte de Service 2009). We thank Dr. Richard Miles for helpful comments on the manuscript.

References

Alexander AS, Nitz DA (2015) Retrosplenial cortex maps the conjunction of internal and external spaces. Nat Neurosci 18:1143–1151.

Auger SD, Mullally SL, Maguire EA (2012) Retrosplenial Cortex Codes for Permanent Landmarks. PLOS ONE 7:e43620.

Balsamo G, Blanco-Hernández E, Liang F, Naumann RK, Coletta S, Burgalossi A, Preston-Ferrer P (2022) Modular microcircuit organization of the presubicular head-direction map. Cell Rep 39.

Blair HT, Sharp PE (1995) Anticipatory head direction signals in anterior thalamus: evidence for a thalamocortical circuit that integrates angular head motion to compute head direction. J Neurosci 15:6260–6270.

Boccara CN, Sargolini F, Thoresen VH, Solstad T, Witter MP, Moser EI, Moser M-B (2010) Grid cells in pre- and parasubiculum. Nat Neurosci 13:987–994.

Calton JL, Stackman RW, Goodridge JP, Archey WB, Dudchenko PA, Taube JS (2003) Hippocampal place cell instability after lesions of the head direction cell network. J Neurosci 23:9719–9731.

Clark BJ, Bassett JP, Wang SS, Taube JS (2010) Impaired Head Direction Cell Representation in the Anterodorsal Thalamus after Lesions of the Retrosplenial Cortex. J Neurosci 30:5289–5302.

Fallahnezhad M, Le Mero J, Zenelaj X, Vincent J, Rochefort C, Rondi-Reig L (2023) Cerebellar control of a unitary head direction sense. Proc Natl Acad Sci U S A 120:e2214539120.

Fisher YE, Marquis M, D'Alessandro I, Wilson RI (2022) Dopamine promotes head direction plasticity during orienting movements. Nature 612:316–322.

Fricker D, Dinocourt C, Eugène E, Wood JN, Wood J, Miles R (2009) Pyramidal cells of rodent presubiculum express a tetrodotoxin-insensitive Na+ current. J Physiol 587:4249–4264.

Gil Z, Connors BW, Amitai Y (1999) Efficacy of thalamocortical and intracortical synaptic connections: quanta, innervation, and reliability. Neuron 23:385–397.

Goodridge JP, Taube JS (1997) Interaction between the postsubiculum and anterior thalamus in the generation of head direction cell activity. J Neurosci 17:9315–9330.

Hedrick NG, Lu Z, Bushong E, Singhi S, Nguyen P, Magaña Y, Jilani S, Lim BK, Ellisman M, Komiyama T (2022) Learning binds new inputs into functional synaptic clusters via spinogenesis. Nat Neurosci 25:726–737.

Huang L-W, Simonnet J, Nassar M, Richevaux L, Lofredi R, Fricker D (2017) Laminar Localization and Projection-Specific Properties of Presubicular Neurons Targeting the Lateral Mammillary Nucleus, Thalamus, or Medial Entorhinal Cortex. eneuro 4:ENEURO.0370-16.2017.

Jacob P-Y, Casali G, Spieser L, Page H, Overington D, Jeffery K (2017) An independent, landmark-dominated head-direction signal in dysgranular retrosplenial cortex. Nat Neurosci 20:173–175.

Jones BF, Witter MP (2007) Cingulate cortex projections to the parahippocampal region and hippocampal formation in the rat. Hippocampus 17:957–976.

Keshavarzi S, Bracey EF, Faville RA, Campagner D, Tyson AL, Lenzi SC, Branco T, Margrie TW (2022) Multisensory coding of angular head velocity in the retrosplenial cortex. Neuron 110:532-543.e9.

Klapoetke NC et al. (2014) Independent optical excitation of distinct neural populations. Nat Methods 11:338–346.

Knierim JJ, Zhang K (2012) Attractor dynamics of spatially correlated neural activity in the limbic system. Annu Rev Neurosci 35:267–285.

Kononenko NL, Witter MP (2012) Presubiculum layer III conveys retrosplenial input to the medial entorhinal cortex. Hippocampus 22:881–895.

Liu J, Kashima T, Morikawa S, Noguchi A, Ikegaya Y, Matsumoto N (2021) Molecular characterization of superficial layers of the presubiculum during development. Front Neuroanat 15.

Mathon B, Nassar M, Simonnet J, Le Duigou C, Clemenceau S, Miles R, Fricker D (2015) Increasing the effectiveness of intracerebral injections in adult and neonatal mice: a neurosurgical point of view. Neurosci Bull 31:685–696.

McNaughton BL, Battaglia FP, Jensen O, Moser EI, Moser M-B (2006) Path integration and the neural basis of the “cognitive map.” Nat Rev Neurosci 7:663–678.

Milstein AD, Bloss EB, Apostolides PF, Vaidya SP, Dilly GA, Zemelman BV, Magee JC (2015) Inhibitory Gating of Input Comparison in the CA1 Microcircuit. Neuron 87:1274–1289.

Nassar M, Simonnet J, Huang L-W, Mathon B, Cohen I, Bendels MHK, Beraneck M, Miles R, Fricker D (2018) Anterior Thalamic Excitation and Feedforward Inhibition of Presubicular Neurons Projecting to Medial Entorhinal Cortex. J Neurosci 38:6411–6425.

Naud R, Friedenberger Z, Toth K (2023) Silences, Spikes and Bursts: Three-Part Knot of the Neural Code.

Payeur A, Guerguiev J, Zenke F, Richards BA, Naud R (2021) Burst-dependent synaptic plasticity can coordinate learning in hierarchical circuits. Nat Neurosci 24:1010–1019.

Peyrache A, Lacroix MM, Petersen PC, Buzsáki G (2015) Internally organized mechanisms of the head direction sense. Nat Neurosci 18:569–575.

Poirazi P, Papoutsi A (2020) Illuminating dendritic function with computational models. Nat Rev Neurosci 1–19.

Polsky A, Mel BW, Schiller J (2004) Computational subunits in thin dendrites of pyramidal cells. Nat Neurosci 7:621–627.

Porter JT, Cauli B, Tsuzuki K, Lambolez B, Rossier J, Audinat E (1999) Selective excitation of subtypes of neocortical interneurons by nicotinic receptors. J Neurosci Off J Soc Neurosci 19:5228–5235.

Preston-Ferrer P, Coletta S, Frey M, Burgalossi A (2016) Anatomical organization of presubicular head-direction circuits. eLife 5.

Ranck JB (1984) Head direction cells in the deep layer of dorsal presubiculum in freely moving rats. Soc Neurosci Abstr.

Rees CL, Moradi K, Ascoli GA (2017) Weighing the Evidence in Peters’ Rule: Does Neuronal Morphology Predict Connectivity? Trends Neurosci 40:63–71.

Richevaux L, Schenberg L, Beraneck M, Fricker D (2019) In Vivo Intracerebral Stereotaxic Injections for Optogenetic Stimulation of Long-Range Inputs in Mouse Brain Slices. JoVE J Vis Exp e59534.

Shibata H, Honda Y (2012) Thalamocortical projections of the anterodorsal thalamic nucleus in the rabbit. J Comp Neurol 520:2647–2656.

Simonnet J, Eugène E, Cohen I, Miles R, Fricker D (2013) Cellular neuroanatomy of rat presubiculum. Eur J Neurosci 37:583–597.

Simonnet J, Nassar M, Stella F, Cohen I, Mathon B, Boccara CN, Miles R, Fricker D (2017) Activity dependent feedback inhibition may maintain head direction signals in mouse presubiculum. Nat Commun 8:16032.

Simonnet J, Richevaux L, Fricker D (2021) Single or Double Patch-Clamp Recordings In Ex Vivo Slice Preparation: Functional Connectivity, Synapse Dynamics, and Optogenetics. Methods Mol Biol Clifton NJ 2188:285–309.

Sit KK, Goard MJ (2022) Coregistration of heading to visual cues in retrosplenial cortex.

Skaggs WE, Knierim JJ, Kudrimoti HS, McNaughton BL (1995) A model of the neural basis of the rat's sense of direction. Adv Neural Inf Process Syst 7:173–180.

Slomianka L, Geneser FA (1991) Distribution of acetylcholinesterase in the hippocampal region of the mouse: I. Entorhinal area, parasubiculum, retrosplenial area, and presubiculum. J Comp Neurol 303:339–354.

Stackman RW, Taube JS (1998) Firing properties of rat lateral mammillary single units: head direction, head pitch, and angular head velocity. J Neurosci 18:9020–9037.

Sugar J, Witter MP (2016) Postnatal development of retrosplenial projections to the parahippocampal region of the rat. eLife 5.

Takahashi N, Oertner TG, Hegemann P, Larkum ME (2016) Active cortical dendrites modulate perception. Science 354:1587–1590.

Taube JS (1995) Head direction cells recorded in the anterior thalamic nuclei of freely moving rats. J Neurosci 15:70–86.

Taube JS, Muller RU, Ranck JB (1990a) Head-direction cells recorded from the postsubiculum in freely moving rats. I. Description and quantitative analysis. J Neurosci 10:420–435.

Taube JS, Muller RU, Ranck JB (1990b) Head-direction cells recorded from the postsubiculum in freely moving rats. II. Effects of environmental manipulations. J Neurosci 10:436–447.

Van der Goes M-SH, Voigts J, Newman JP, Toloza EHS, Brown NJ, Murugan P, Harnett MT (2022) Coordinated Head Direction Representations in Mouse Anterodorsal Thalamic Nucleus and Retrosplenial Cortex.

Van Groen T, Wyss JM (2003) Connections of the retrosplenial granular b cortex in the rat. J Comp Neurol 463:249–263.

Van Groen T, Wyss JM (1992) Connections of the retrosplenial dysgranular cortex in the rat. J Comp Neurol 315:200–216.

Van Groen T, Wyss JM (1990a) The connections of presubiculum and parasubiculum in the rat. Brain Res 518:227–243.

Van Groen T, Wyss JM (1990b) Connections of the retrosplenial granular a cortex in the rat. J Comp Neurol 300:593–606.

Van Groen T, Wyss JM (1990c) The postsubicular cortex in the rat: characterization of the fourth region of the subicular cortex and its connections. Brain Res 529:165–177.

Vogt BA, Miller MW (1983) Cortical connections between rat cingulate cortex and visual, motor, and postsubicular cortices. J Comp Neurol 216:192–210.

Yoder RM, Peck JR, Taube JS (2015) Visual landmark information gains control of the head direction signal at the lateral mammillary nuclei. J Neurosci 35:1354–1367.

Yoder RM, Taube JS (2011) Projections to the anterodorsal thalamus and lateral mammillary nuclei arise from different cell populations within the postsubiculum: implications for the control of head direction cells. Hippocampus 21:1062–1073.

Yoder RM, Valerio S, Crego ACG, Clark BJ, Taube JS (2019) Bilateral postsubiculum lesions impair visual and nonvisual homing performance in rats. Behav Neurosci 133:496–507.

Zugaro MB, Arleo A, Berthoz A, Wiener SI (2003) Rapid spatial reorientation and head direction cells. J Neurosci 23:3478–3482.